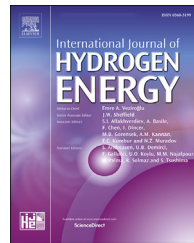




ELSEVIER

Available online at [www.sciencedirect.com](http://www.sciencedirect.com)

ScienceDirect

journal homepage: [www.elsevier.com/locate/he](http://www.elsevier.com/locate/he)

# Carbon supported nickel phosphide as efficient electrocatalyst for hydrogen and oxygen evolution reactions

Premnath Kumar <sup>a,1</sup>, Arun Prasad Murthy <sup>b,1</sup>, Leticia S. Bezerra <sup>c,1</sup>, Bibiana K. Martini <sup>c,1</sup>, Gilberto Maia <sup>c,\*</sup>, Jagannathan Madhavan <sup>a,\*\*</sup>

<sup>a</sup> Solar Energy Lab, Department of Chemistry, Thiruvalluvar University, Vellore, 632115, Tamil Nadu, India

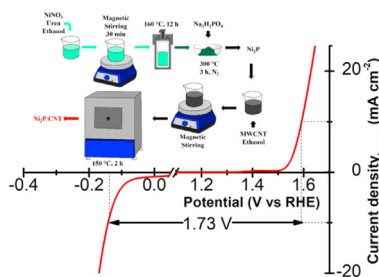
<sup>b</sup> Department of Chemistry, School of Advanced Sciences, Vellore Institute of Technology (VIT), Vellore, 632 014, Tamil Nadu, India

<sup>c</sup> Institute of Chemistry, Federal University of MatoGrosso Do Sul; Av. Senador Filinto Muller, 1555; Campo Grande, 79074-460, MS, Brazil

## HIGHLIGHTS

- Simplest solvothermal route was used to produce Ni<sub>2</sub>P and Ni<sub>2</sub>P/CNT.
- Ni<sub>2</sub>P/CNT showed higher activity toward HER and OER.
- Ni<sub>2</sub>P/CNT can be used as a platinum-free electrocatalyst.
- Ni<sub>2</sub>P/CNT can be used as an alternative for water splitting process.

## GRAPHICAL ABSTRACT



## ARTICLE INFO

### Article history:

Received 16 June 2020

Received in revised form

28 September 2020

Accepted 30 September 2020

Available online 21 October 2020

## ABSTRACT

Hydrogen production through water splitting is an efficient and green technology for fulfilling future energy demands. Carbon nanotubes (CNT) supported Ni<sub>2</sub>P has been synthesized through a simpler hydrothermal method. Ni<sub>2</sub>P/CNT has been employed as efficient electrocatalysts for hydrogen and oxygen evolution reactions in acidic and alkaline media respectively. The electrocatalyst has exhibited low overpotential of 137 and 360 mV for hydrogen and oxygen evolution reactions respectively at 10 mA cm<sup>-2</sup>. Lower Tafel slopes, improved electrochemical active surface area, enhanced stability have also been observed.

\* Corresponding author.

\*\* Corresponding author.

E-mail addresses: [gilberto.maia@ufms.br](mailto:gilberto.maia@ufms.br), [gilberto.maia@pq.cnpq.br](mailto:gilberto.maia@pq.cnpq.br) (G. Maia), [jagan.madhavan@gmail.com](mailto:jagan.madhavan@gmail.com) (J. Madhavan).

<sup>1</sup> These authors contributed equally to this work.

**Keywords:**  
 Water splitting  
 Nickel phosphide  
 Carbon nanotubes  
 Hydrogen evolution reaction  
 Oxygen evolution reaction

Advantages of carbon support in terms of activity and stability have been described by comparing with unsupported electrocatalyst.

© 2020 Hydrogen Energy Publications LLC. Published by Elsevier Ltd. All rights reserved.

## Introduction

The renewable energy supply is important to realization of sustainable human society of near future. Furthermore, environment pollution due to combustion of fossil fuels adds to the energy crisis. In this context, hydrogen, widely considered as green energy capable of meeting the demands of future energy needs, can be electrochemically produced with zero carbon emission. Hydrogen with high energy density of 142 MJ kg<sup>-1</sup> can be ideal green fuel when produced from renewable and sustainable energy sources [1–6]. For example, intermittent wind or solar energy is one of the most efficient and sustainable routes for producing high-purity hydrogen through water splitting [7–14]. The water splitting reaction consists of two half-reactions, viz., cathodic hydrogen evolution reaction, HER [15].



and anodic oxygen evolution reaction, OER



The hydrogen evolution reaction (HER) is effectively facilitated by noble metals such as Pt, RuO<sub>2</sub>, which generate large cathodic current densities for this reaction at low overpotentials [16]. Platinum is the most active electrocatalyst for cathodic half-reaction of HER and ruthenium dioxide and iridium dioxide are most efficient for anodic half-reaction of OER. However, these catalysts are scarce and expensive hence cannot be viable for large-scale production of hydrogen [17–20].

Over the past decades, many low-cost earth abundant transition metals based materials have been developed and employed as HER and OER electrocatalysts [21,22]. Recently, transition metal phosphides (TMPs) have attracted much attention as promising HER/OER electrocatalysts [23]. TMPs possess desirable electrocatalytic properties, metalloid characteristics and significant earth abundance. In this context, classes of transition metal chalcogenides (metal phosphides) have been revealed as outstanding electrocatalysts for HER/OER activity which is possibly due to their higher electrocatalytic activity, low cost, more abundance and unique crystal structure.

As the platinum free noble-metal electrocatalysts, TMPs such as Ni<sub>2</sub>P [24], CoP [25], NiCoP [26], FeP [27], Cu<sub>3</sub>P [28], MoP [29], Ni<sub>12</sub>P<sub>5</sub> [30], Co<sub>2</sub>P [31] have proven to be high efficient electrocatalyst for HER. Nickel phosphides of several shapes, sizes and hetero structures have been fabricated for OER electrocatalyst such as Ni<sub>2</sub>P nanowires and polydispersed

Ni<sub>2</sub>P nanoparticles [32], oxygen-incorporated Ni<sub>2</sub>P nanosheet [33], porous multishelled Ni<sub>2</sub>P hollow microspheres [34], nickel phosphides porous nanoplates with mixed phases of Ni<sub>5</sub>P<sub>4</sub> and Ni<sub>2</sub>P [35], self-supported 3D carbon fiber paper (CP) electrode [36], three-dimensional porous nickel phosphide (Ni–P) foam with Ni<sub>2</sub>P skeletons covered with vertically aligned Ni<sub>5</sub>P<sub>4</sub>–NiP<sub>2</sub> nanosheets [37], Ni<sub>2</sub>P nanocrystals supported on a graphene (Ni<sub>2</sub>P@C/G) [38], tri-metallic phosphide FeCoNiP [39], three-dimensional honeycomb monolithic catalysts consisting of macroporous Ni<sub>2</sub>P coated on nickel foam [40] etc. The additive of carbon in the form of support improves the catalytic activity by increasing surface area, exposing more active sites, improving electric conductivity, enhancing long-term stability, etc [41]. Additionally, as compared with other representative carbon materials (carbon black (C) and carbon nanotubes (CNTs)) in the perspective of specific surface area (SSA), conductivity and electronic interaction to TMS [42]. When the nickel phosphide NPs is supported in CNT, the electrical conductivity of catalyst can be improved [43]. In the present investigation, we adopted solvothermal process followed by phosphidation to prepare Ni<sub>2</sub>P and it was composited with carbon nanotubes (Ni<sub>2</sub>P/CNT) and employed as efficient HER and OER electrocatalyst in acid and alkaline media respectively. This non-noble metal electrocatalyst was synthesized through a simple low-cost method and exhibited low overpotential ( $\eta_{10}$ ) of 137 and 360 mV for HER and OER respectively at 10 mA cm<sup>-2</sup>.

## Experimental section

### Synthesis of Ni<sub>2</sub>P

The electrochemical active Ni<sub>2</sub>P was synthesized by the phosphidation of the nickel oxide prepared via solvothermal process, using 0.5 mmol of nickel nitrate, 0.5 mmol of urea dissolved in 30 mL ethanol, solution was stirred well under magnetic agitation for 30 min after that solution was transfer into Teflon-lined autoclave to carry out the solvothermal reaction at 160 °C for 12 h. The precipitation solution was filtered, washed with ethanol several times, and then the obtained precipitate was dried out at 60 °C for 6 h. This precursor and Na<sub>2</sub>H<sub>2</sub>PO<sub>4</sub> both are grained well then placed out in a quartz boat, the phosphidation process was carried out under N<sub>2</sub> flowing at 300 °C for 3 h (Scheme 1). After the phosphidation process the boat was cooled down to room temperature grained well then collected for characterization of Ni<sub>2</sub>P nano particle, the electrochemical analyses were carried out for HER and OER.

### Synthesis of Ni<sub>2</sub>P/CNT

100 mg of as-prepared Ni<sub>2</sub>P was taken with 30 mg of MWCNT in 30 mL of ethanol and were magnetically stirred well before drying at 60 °C for 1 h. The 30% incorporated CNT with Ni<sub>2</sub>P was annealed at 150 °C in muffle furnace for 2 h (Scheme 1).

### Material characterization

The prepared electrocatalyst were characterized by the following techniques, X-ray diffraction spectroscopy (XRD) recorded by using Rigaku Mini Flex II with Cu K $\alpha$  irradiation ( $\lambda = 1.5406 \text{ \AA}$ ) in 20 range of 20–80° at 4°/min. The surface morphologies of the samples can be assessed by a scanning electron microscopy (SEM, Hitachi S-4700, Japan) and a JEM-2100F high-resolution transmission electron microscope (HR-TEM, JEOL Ltd., Japan). The elemental composition study was derived from EDS (Oxford X-Act). The X-ray excited photoelectron spectroscopy (XPS) analysis was conducted in an Omicron surface analysis station equipped with a SPHERA hemispherical analyser and an X-ray source DAR 400 K $\alpha$  (1486.7 eV) by using the conditions of 50 eV pass energy for survey spectra and 10 eV pass energy for high resolution, and keeping the chamber evacuated to a base pressure of  $1 \times 10^{-8} \text{ mbar}$ . The Voigt-type function with Gaussian (70%) and Lorentzian (30%) combinations was used for deconvolute the high resolution HR-XPS spectra.

### Electrochemical analysis

An AFP2 WAVEDRive 20 bipotentiostat–galvanostat coupled to an AFMSRCE modulated speed rotator from Pine Research Instrumentation was used for cyclic voltammetry and linear sweep voltammetry. All experiments were conducted in a

standard three-electrode system, using graphite and a reversible hydrogen electrode (directly) as counter and reference electrodes, respectively. A carbon paper (CP) and a glassy carbon (GC) disk/Pt ring embedded in Teflon (geometric area = 0.196 and 0.11 cm<sup>2</sup>, respectively, with a collection efficiency of N = 0.26 – Pine Research Instrumentation) were used as working electrodes. Stability experiments for OER were performed by chronoamperometry during 22 h in KOH 1 M, O<sub>2</sub>–saturated at the potential that matches 10 mA cm<sup>-2</sup> of current density. Electrochemical impedance spectroscopy and capacitance of double-layer ( $C_{DL}$ ) were evaluated using a PGSTAT128 N potentiostat–galvanostat (Auto lab) equipped with a FRA2.X module in KOH 1 M, N<sub>2</sub>–saturated solution. The double-layer capacitance was measured by cyclic voltammetry at several scans rates (5; 10; 15; 20; 30; 40; 60 and 80 mV s<sup>-1</sup>) with a potential window of 100 mV with open circuit potential centered. The following relation was applied for the calculation of  $C_{DL}$  [44]. The current densities are obtained by using the electrodes geometric area.

$$I = C_{DL} \cdot v \quad (3)$$

where,

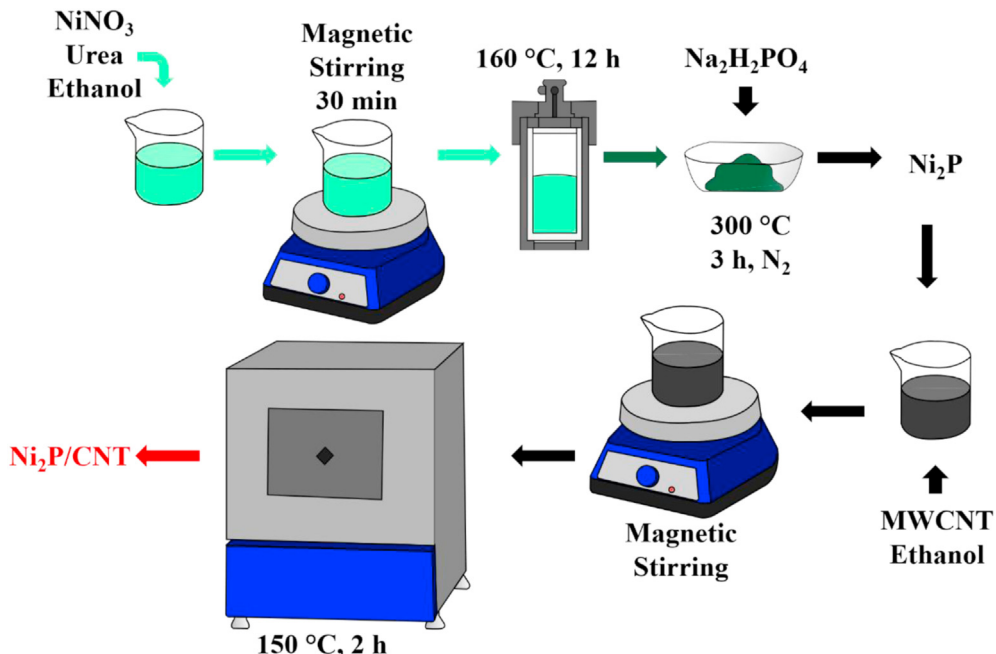
I is the current (A),  $C_{DL}$  is the capacitance of double-layer (F cm<sup>-2</sup>) and v (V s<sup>-1</sup>). Electrochemical surface active area (ECSA) could be calculated by the following relation:

$$\text{ECSA} = \frac{C_{DL}}{C_s} \quad (4)$$

where.

$C_s$  is the specific capacitance ( $4.10^{-5} \text{ F cm}^{-2}$ ) [44].

The CP was cleaned using ultrasonic bath with deionized water 10 times. The materials were dispersed in ultrapure water to produce a catalyst ink with a concentration of 1 mg mL<sup>-1</sup>. An aliquot of such catalyst ink was drop cast on



Scheme 1 – Summary of the synthesis of Ni<sub>2</sub>P and Ni<sub>2</sub>P/CNT catalysts.

the surface of the precleaned CP (or GC) electrode to achieve a content of  $150 \mu\text{g cm}^{-2}$  and dried at room temperature. The analyses were carried out in 0.5 M  $\text{H}_2\text{SO}_4$  and 1 M KOH electrolytes for HER and OER respectively.

## Results and discussion

### Physical characterization

**Fig. 1** shows the XRD patterns of as-synthesized  $\text{Ni}_2\text{P}$  and  $\text{Ni}_2\text{P}/\text{CNT}$  along with that of CNT. Prominent peaks appear at  $2\theta = 15.3, 27.0, 30.4, 40.7, 44.5, 47.3, 53.0, 66.3$  and  $76.1^\circ$ . These peaks are consistent with the hexagonal phase of  $\text{Ni}_2\text{P}$  corresponding to (100), (110), (201), (210), (211), (310) and (212) planes of  $\text{Ni}_2\text{P}$  (JCPDS No. 74–1385) and peaks at 26.3, 44.6 and 66.3 corresponding to (001), (201) and (202) planes of CNT. A good match between the patterns of as-synthesized samples and the standard reference can be observed in the figure. The above data confirms the successful formation of  $\text{Ni}_2\text{P}$  and  $\text{Ni}_2\text{P}/\text{CNT}$  with high phase purity. The particle sizes of the catalysts were calculated using Scherr's equation as noted in **Table 1**. The crystallite size of  $\text{Ni}_2\text{P}$  at  $\text{Ni}_2\text{P}/\text{CNT}$  nanocomposite (24.9 nm) was decreased in relation to  $\text{Ni}_2\text{P}$  (31.2 nm). **Fig. 2** shows SEM images characterizing the morphologies of  $\text{Ni}_2\text{P}$  and  $\text{Ni}_2\text{P}/\text{CNT}$ . In the figure, flower-like structures of  $\text{Ni}_2\text{P}$  could be observed which is typical of the products obtained from hydrothermal synthesis method [8]. As well, the flower-like structures of  $\text{Ni}_2\text{P}$  appeared nanocomposited to the CNTs. A good electrocatalytic HER and OER performance can be expected from the highly connected nanostructure as well as the formed nanocomposite as shown in the figure.

**Fig. 3** shows the EDS spectra images for (a) pure  $\text{Ni}_2\text{P}$  and (b)  $\text{Ni}_2\text{P}/\text{CNT}$  composite. The EDS spectroscopy confirms the elements present in the  $\text{Ni}_2\text{P}$  and  $\text{Ni}_2\text{P}/\text{CNT}$  composite, and the atomic ratio for these materials are also mentioned in **Fig. 3** (a,b). The EDS clearly illustrate the presence of carbon between  $\text{Ni}_2\text{P}$  (**Fig. 3b**), no other impurity peaks are observed and

the atomic percentage of the elements are also mentioned in the figure. TEM images for the electrocatalyst were collected to investigate the morphological structure as shown in **Fig. 4(a-d)**. It can be noted that  $\text{Ni}_2\text{P}$  exhibits uniform nanoflower-like morphology and also incorporated CNTs are visible on  $\text{Ni}_2\text{P}/\text{CNT}$  nanocomposite (**Fig. S1a**). Well-resolved lattice fringes with interplanar distance of 0.29 nm and 0.56 nm (**Fig. 4** and **Fig. S1b**) corresponded to the (100) [34] and (100) [32,38] facets of  $\text{Ni}_2\text{P}$  crystal planes.

**Fig. S2** shows the XPS survey spectra for the synthesized catalysts before and after OER stability test. The XPS survey spectra (**Fig. S2**) show the peaks related to Ni, C, and O, with P really visible to  $\text{Ni}_2\text{P}$  before OER stability test and Ni not visible to  $\text{Ni}_2\text{P}$  after OER stability test. It is important to inform that to obtain the XPS spectra the catalysts were supported in CP. The atomic percentage content for C 1s is high and for oxygen O 1s is low when  $\text{Ni}_2\text{P}/\text{CNT}$  is compared with  $\text{Ni}_2\text{P}$  (**Table S1**) reinforcing the presence of CNT in  $\text{Ni}_2\text{P}/\text{CNT}$ . The atomic percentage content for P 2p (5.6%) is detected only to  $\text{Ni}_2\text{P}$  and the atomic percentage content for Ni 2p is not so different between the two catalysts (in average 1.1%, **Table S1**). Most probable P is the linker of  $\text{Ni}_2\text{P}$  with the CNT, not remaining at the surface and being not visible for XPS measurements.

After OER stability test the atomic percentage contents for C 1s, O 1s, and Ni 2p for  $\text{Ni}_2\text{P}/\text{CNT}$  can be considered equal to before OER stability test (compare **Tables S2 and S1**). However, in the case of  $\text{Ni}_2\text{P}$  the Ni 2p and P 2p are not detected anymore and the atomic percentage contents for C 1s and O 1s are enough modified (**Table S2**), suggesting the detachment of  $\text{Ni}_2\text{P}$  from the CP surface after OER stability test.

**Fig. 5** and **Fig. S3** show the high resolution XPS (HR-XPS) spectra for Ni 2p, P 2p, C 1s, and O 1s regions for the synthesized catalysts before and after OER stability test. The Ni 2p HR-XPS spectra (**Fig. 5**) contain two peaks with their respective satellite shake-ups related to  $2p_{3/2}$  and  $2p_{1/2}$  respectively [6,45] (see their positions and % contents in **Tables S3 and S4**). There are not many differences between the % content for different Ni groups comparing  $\text{Ni}_2\text{P}/\text{CNT}$  before and after OER stability test with  $\text{Ni}_2\text{P}$  before OER stability test (**Tables S3 and S4**). However, HR-XPS signal for Ni 2p was not detected for  $\text{Ni}_2\text{P}$  after OER stability test (**Fig. 5**) suggesting the detachment and instability of this material at CP surface after OER stability test. The  $\text{Ni}_2\text{P}/\text{CNT}$  was stable at CP surface after OER stability test (**Fig. 5**).

The HR-XPS signal for P 2p was detected only to  $\text{Ni}_2\text{P}$  before OER stability test (**Fig. 5**) which the peak at 133.8 eV (**Table S3**) can be attributed to oxidized P species due the exposition of  $\text{Ni}_2\text{P}$  to air [46]. The absence of HR-XPS P 2p signal for  $\text{Ni}_2\text{P}$  after OER stability test (**Fig. 5**) is attributed to the detachment of

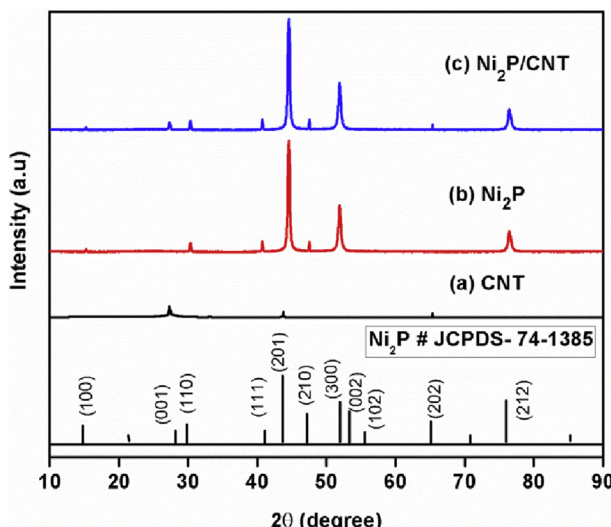


**Fig. 1 – XRD patterns of (a) CNT, (b)  $\text{Ni}_2\text{P}$  and (c)  $\text{Ni}_2\text{P}/\text{CNT}$ .**

**Table 1 – The electrochemical parameters of the  $\text{Ni}_2\text{P}$  and  $\text{Ni}_2\text{P}/\text{C}$  Composites.**

Sample	HER $\eta_{10}$ (mV)	HER Tafel slope (mV dec <sup>-1</sup> )	OER $\eta_{10}$ (mV)	OER Tafel slope (mV dec <sup>-1</sup> )	Crystallite size (nm)
$\text{Ni}_2\text{P}$	185	96.5	390	55	31.23
$\text{Ni}_2\text{P}/\text{CNT}$	137	71.3	360	49	24.88

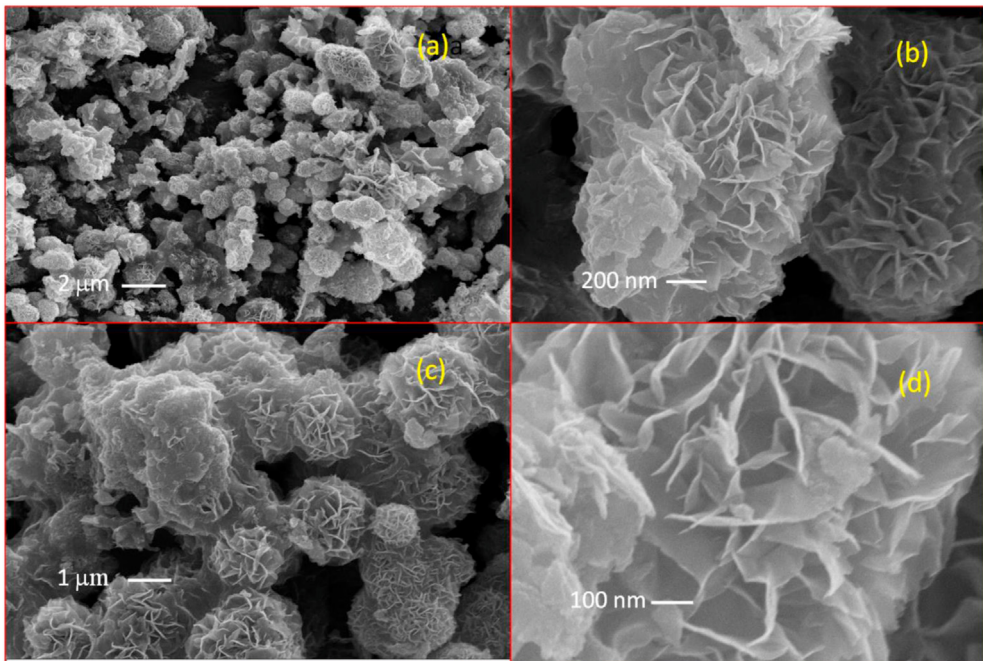


**Fig. 2 – SEM images of as synthesized Ni<sub>2</sub>P (a–d).**

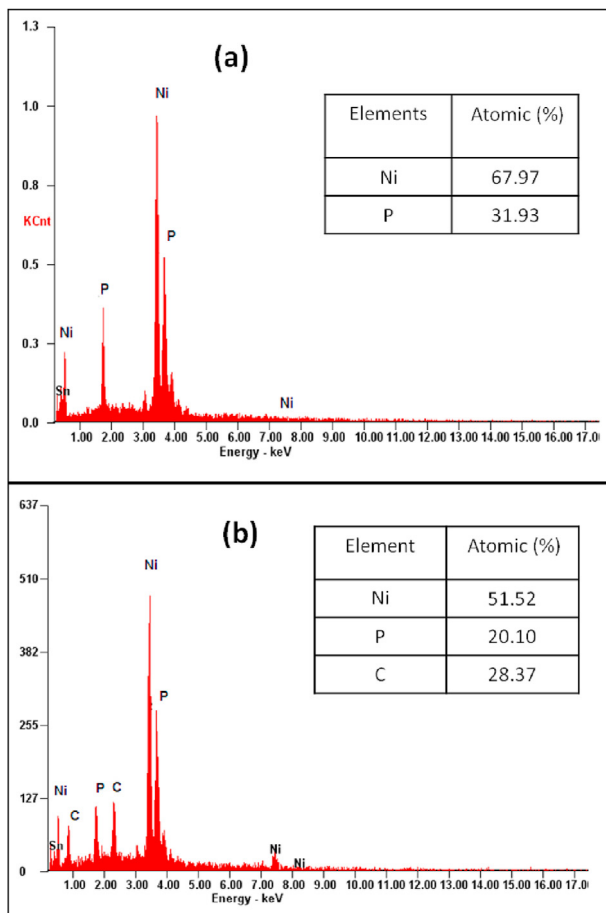


**Fig. 3 – EDS images of the as prepared (a) Ni<sub>2</sub>P and (b) Ni<sub>2</sub>P/CNT.**

Ni<sub>2</sub>P from the CP surface. For Ni<sub>2</sub>P/CNT before and after OER stability test, the absence of HR-XPS P 2p signal (Fig. 5) is attributed to the link of P with CNT, resting XPS visible only Ni atoms at Ni<sub>2</sub>P linked to CNT surface.

The HR-XPS spectra for C 1s (Fig. 5 and Fig. S3) are quite similar between the different samples with the deconvolution attribution for the different groups and positions (Tables S3 and S4) in agreement with the literature [45,47–51] and the % content to C=C and C–C groups 10% higher for Ni<sub>2</sub>P before and after OER stability test in comparison with Ni<sub>2</sub>P/CNT before and after OER stability test (Tables S3 and S4). This difference in % content to C=C and C–C groups suggest the detection of CNT in the case of Ni<sub>2</sub>P/CNT before and after OER stability test and CP surface.

The deconvoluted HR-XPS spectra for O 1s (Fig. 5 and Fig. S3) are related to different groups and positions (Tables S3 and S4), in agreement with the literature [45,47–51]. However, the presence of Ni–O group at Ni<sub>2</sub>P/CNT before and after OER stability test samples and the decrease of the % content of this group at Ni<sub>2</sub>P/CNT after OER stability test samples (Tables S3 and S4), reinforces the link of Ni<sub>2</sub>P with CNT and Ni is less oxidized after OER stability test, suggesting better stability of Ni<sub>2</sub>P/CNT toward OER. For Ni<sub>2</sub>P before OER stability test appears the oxidized P group (O–P) and after OER stability test the C=O group increased enough its % content (Tables S3 and S4), reinforcing the strong detachment of Ni<sub>2</sub>P from the CP surface.

#### HER activities of nickel phosphides

Glassy carbon electrodes modified with Ni<sub>2</sub>P and Ni<sub>2</sub>P/CNT were subjected to voltammetric analysis in a three-electrode cell with 0.5 M H<sub>2</sub>SO<sub>4</sub> electrolyte. Fig. 6a shows polarization curves exhibiting the HER activities of the electrocatalysts at

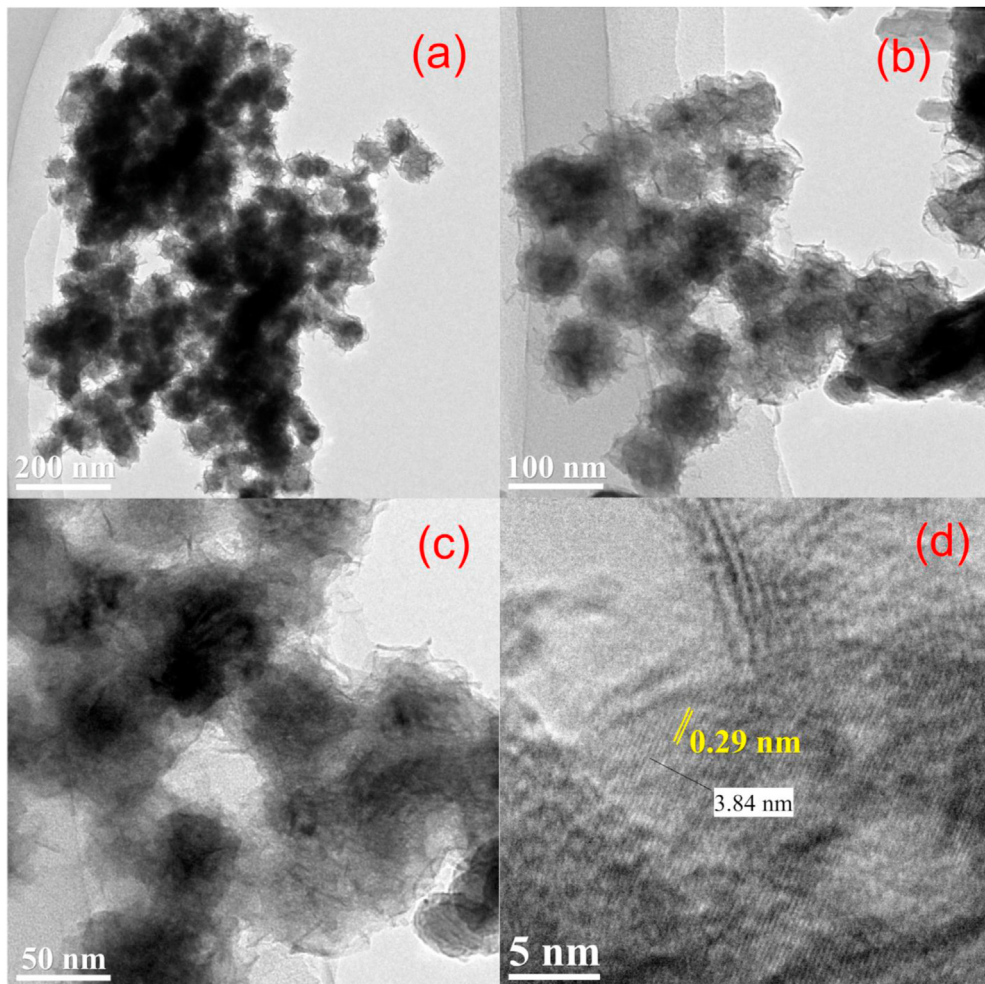


**Fig. 4 – TEM images of as prepared Ni<sub>2</sub>P electrocatalyst. The sized line reveals the lattice fringes. The interplanar distance is 0.29 nm.**

5 mV s<sup>-1</sup> scan rate. To evaluate the catalytic performance of various electrocatalysts, the overpotential at current density of 10 mA cm<sup>-2</sup> ( $\eta_{10}$ ) (corresponding to water splitting with 10% solar-to-hydrogen efficiency under one sun illumination [52]) was measured. As can be seen in Fig. 6a, Ni<sub>2</sub>P achieved  $\eta_{10}$  of 185 mV expected of an unsupported electrocatalyst while Ni<sub>2</sub>P/CNT recorded lower  $\eta_{10}$  of 137 mV and the bare glassy carbon electrode showed negligible activity under the same experimental conditions (data not shown). The better HER activity of Ni<sub>2</sub>P/CNT over Ni<sub>2</sub>P shows the beneficial contribution of CNT that could be understood in terms of lowering of electronic resistance due to the presence of CNT [22]. To compare the Ni<sub>2</sub>P/CNT catalytic activity with commercial Pt(20%)C the polarization curve was recorded for Pt(20%)C electrode [53] as shown in Fig. 6a, in which case Pt(20%)C achieved 35 mV of overpotential at  $\eta_{10}$ . The results clearly illustrate that the as synthesized Ni<sub>2</sub>P/CNT exhibits the enhanced electrochemical activity as much near to the Pt performance. Tafel analysis of the voltammetric data would reveal the mechanistic aspects of HER by plotting overpotential ( $\eta$ ) against the logarithm of current density ( $j$ ), as shown in Fig. 6b. The linear part of the Tafel plot was fitted

with the Tafel equation, ( $\eta = b \log (j) + a$ , where  $b$  and  $a$  represent Tafel slope and constant respectively) to obtain Tafel slope [41,54]. Ni<sub>2</sub>P and Ni<sub>2</sub>P/CNT exhibited Tafel slopes of 96.5 and 71.3 mV dec<sup>-1</sup> respectively, finally the measured Tafel slope value of the Pt(20%)C electrode is 30 mV dec<sup>-1</sup>(data not shown) which is in agreement with the reported values [55]. Ni<sub>2</sub>P/CNT exhibited smaller Tafel slope and the Tafel slope values of both the electrocatalysts fall between 40 and 120 mV dec<sup>-1</sup> indicating Volmer-Heyrovsky as the probable HER mechanism [56].

EIS analysis is widely used as a reliable method to evaluate charge transfer resistance ( $R_{ct}$ ) of an electrochemical reaction between the catalyst and liquid junction (i.e. surface reaction). Fig. 6c shows Nyquist plots of Ni<sub>2</sub>P/CNT and Ni<sub>2</sub>P measured at 10 mV between 1 Hz and 200 kHz in 0.5 M H<sub>2</sub>SO<sub>4</sub>. The Nyquist plots are characterized by single semicircles that can be fitted with Randles equivalent circuit as shown in the figure.  $R_{ct}$  values obtained for Ni<sub>2</sub>P and Ni<sub>2</sub>P/CNT are 783 and 87 Ω respectively. The lower the  $R_{ct}$  values the faster is the reaction kinetics [33]. The Ni<sub>2</sub>P/CNT electrode shows the smallest diameter of semicircle in the Nyquist plot, indicating the minimum charge transfer resistance and superior charge

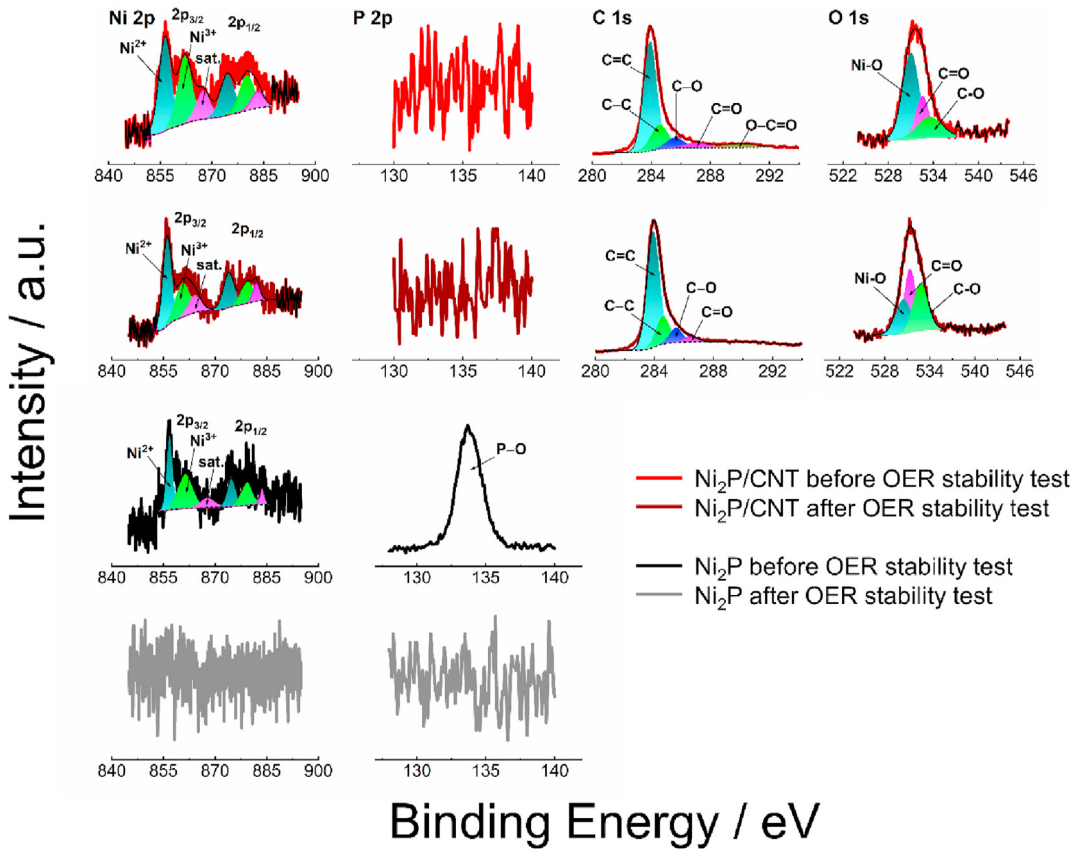


Fig. 5 – High resolution XPS of Ni 2p, P 2p, C 1s, and O 1s regions for the synthesized catalysts before and after OER stability test.

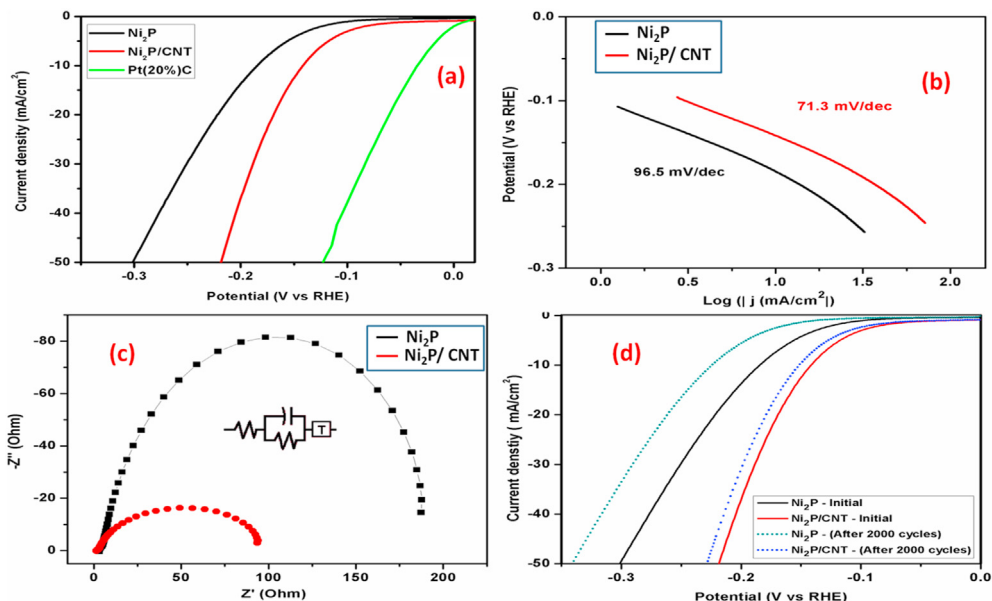


Fig. 6 – a) The Polarization curves showing HER activities of  $\text{Ni}_2\text{P}$ ,  $\text{Ni}_2\text{P}/\text{CNT}$  and Pt(20%)C, in 0.5 M  $\text{H}_2\text{SO}_4$  at a scan rate of 5 mV s<sup>-1</sup>. b) Respective Tafel plots of  $\text{Ni}_2\text{P}$  and  $\text{Ni}_2\text{P}/\text{CNT}$ . c) Nyquist plots of the  $\text{Ni}_2\text{P}/\text{CNT}$  and  $\text{Ni}_2\text{P}$  along with Randles equivalent circuit. d) Voltammograms of  $\text{Ni}_2\text{P}/\text{CNT}$  and  $\text{Ni}_2\text{P}$  before and after accelerated degradation tests.

transport kinetics [57]. Hence HER at  $\text{Ni}_2\text{P}/\text{CNT}$  to be facilitated compared to  $\text{Ni}_2\text{P}$ . The stability of the synthesized electro-catalysts was tested using cyclic voltammetry employing accelerated degradation test.  $\text{Ni}_2\text{P}/\text{CNT}$  and  $\text{Ni}_2\text{P}$  catalysts

were cycled for 2000 times at a scan rate of 50 mV s<sup>-1</sup> in 0.5 M  $\text{H}_2\text{SO}_4$  and the results are shown in Fig. 6d. Initial and final polarization curves are shown in the figure and considerable loss in the activity can be observed for  $\text{Ni}_2\text{P}$ . While in

the case of Ni<sub>2</sub>P/CNT the loss in the activity is about 3% of the initial value. The above data proves that carbon based supports increase the stability of the electrocatalysts compared to catalysts without carbon support [41].

### OER activities of nickel phosphides

Cyclic voltammetric studies were conducted on the modified electrodes of samples Ni<sub>2</sub>P/CNT and Ni<sub>2</sub>P as shown in Fig. S4 and no redox peaks were noticed indicating the absence of redox process. As can be seen in the figure, only capacitive current densities were present in the potential window investigated. In order to investigate the catalytic activity towards OER, the modified electrodes were submitted to hydrodynamic linear voltammetry (HLV) or stationary linear voltammetry (SLV, only when using CP as a substrate) in the potential range of 1.0–1.8 V (Fig. 7a). The bare CP and GC electrodes (Fig. 7a) do not exhibit good catalytic performance toward OER, with low currents and high overpotential values.

The results obtained for Ni<sub>2</sub>P/CNT/GC, Ni<sub>2</sub>P/CNT/CP, and Ni<sub>2</sub>P/GC electrodes were promising with  $\eta_{10}$  values of 360, 370 mV, and 390 mV, respectively (Table S4). Ni<sub>2</sub>P/CNT/GC and Ni<sub>2</sub>P/GC also provided large current densities (76.85 mA and 82.50 mA, respectively) and at 1.8 V Ni<sub>2</sub>P/CNT/GC electrode presented the best OER catalytic response in terms of  $\eta_{10}$  [58]. The no use of ohmic drop compensation to avoid distortion of HLV and SLV responses to OER catalysis results in quite good catalytic activity comparable with other materials [59]. On the other hand, RuO<sub>2</sub>/CP electrode showed low activity, even though RuO<sub>2</sub> being known as the state-of-the-art catalyst for OER [60]. The material of the substrate electrode can directly affect the results obtained during the studies of a new catalyst [61]. Difference in  $\eta_{10}$  for the Ni<sub>2</sub>P/CNT/GC and Ni<sub>2</sub>P/CNT/CP electrodes, as shown in Fig. 7a, could be related to physical characteristics of the substrates and their interaction with the catalysts. Therefore, the best OER activity for the catalysts at GC substrate in relation to CP substrate should be related for the better dispersion and electrical contact between the catalysts and the substrate surface. It may be noted that the onset potential for both Ni<sub>2</sub>P/CNT/GC and Ni<sub>2</sub>P/CNT/CP electrodes are close, suggesting a similar intrinsic activity [62].

Tafel plot (Fig. 7b) is widely applied on the investigation of reaction mechanisms and the rate determining steps through a linear correlation between the logarithmic of the current and the overpotential. Nevertheless, the Tafel equation shouldn't be used to describe the pathway of electrochemical reactions containing several steps, considering the dependence on factors such as intermediate species, coverage, solvent or surface defects [63,64]. For the Ni<sub>2</sub>P/CNT/CP, Ni<sub>2</sub>P/CNT/GC, Ni<sub>2</sub>P/GC, and RuO<sub>2</sub>, the Tafel slopes of 105 mV dec<sup>-1</sup>, 49 mV dec<sup>-1</sup>, 55 mV dec<sup>-1</sup>, and 135 mV dec<sup>-1</sup>, respectively were obtained indicating different rate determining steps among the materials and also could be associated with the number of active sites [65]. However, these Tafel slopes suggest that the number of electrons transferred during the rate determining step for OER is between 1 and 4 electrons 105 and 49 mV dec<sup>-1</sup>, respectively [66]. Electrochemical active surface area (ECSA) for each catalyst was evaluated considering its relation with the catalyst activity, since the OER occurs especially at the active sites [8]. For the Ni<sub>2</sub>P/CNT/GC electrode the ECSA values were higher, resulting in better catalytic response for this electrode (Table S4). (For more information regarding measurements/calculations to obtain ECSA values, see Figs. S7–8.)

To examine the stability of various electrodes investigated under the harsh OER conditions, the modified electrodes were submitted to chronoamperometric studies for a duration of 22 h at the potentials necessary to achieve  $j = 10 \text{ mA cm}^{-2}$  (Fig. S9). The activity of Ni<sub>2</sub>P/CNT/GC decreased after 9 h of the stability test (Fig. S10), with the overpotential starting at 360 mV ( $t = 0 \text{ h}$ ) and ending with 460 mV ( $t = 22 \text{ h}$ ). The above observation demonstrated that the Ni<sub>2</sub>P/CNT/GC is not stable for OER on the GC electrode. For the Ni<sub>2</sub>P/CNT/CP electrode, the activity loss was also observed, beginning with 370 mV of overpotential ( $t = 0 \text{ h}$ ) and ending with 430 mV ( $t = 22 \text{ h}$ ). Because of the porous structure of the carbon paper the release of O<sub>2</sub> gas bubbles are easier compared to the glassy carbon, relieving active sites faster and avoiding the detachment of catalyst particles from the electrode surface. It can explain the better stability of the Ni<sub>2</sub>P/CNT/CP electrode although the Ni<sub>2</sub>P/CNT/GC electrode initially presented best activity toward OER. The Ni<sub>2</sub>P/CNT/GC and Ni<sub>2</sub>P/CNT/CP electrodes presented a decrease in the charge transfer resistance after the stability test experiment (Fig. S11). The charge

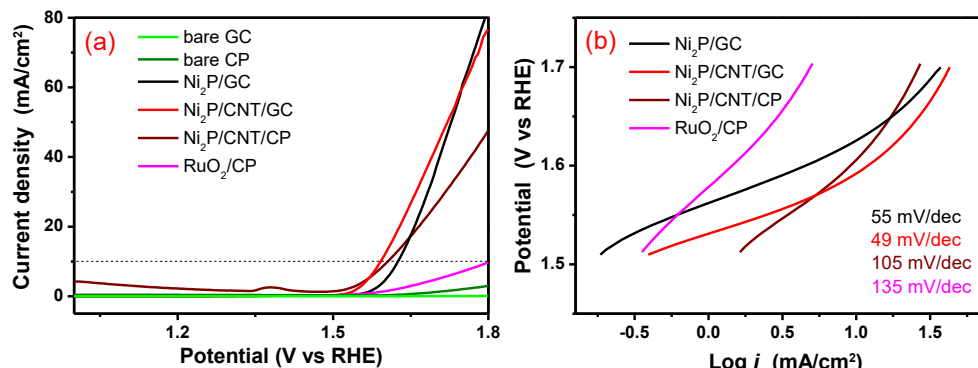


**Fig. 7 – (a)** Hydrodynamic linear voltammograms for the different bare and modified electrodes investigated (stationary linear voltammetry was applied only when CP was used as substrate) using O<sub>2</sub>-saturated 1 M KOH. Potential scan rate: 5 mV s<sup>-1</sup>, starting at 1.0 V. For GC electrodes  $\omega = 1600 \text{ rpm}$ . **(b)** Tafel plots for Ni<sub>2</sub>P/CNT/CP, Ni<sub>2</sub>P/CNT/GC, Ni<sub>2</sub>P/GC, and RuO<sub>2</sub>/CP electrodes. Contents of 150  $\mu\text{g cm}^{-2}$ .

transfer resistance should be decreased in the course of these experiments. The Ni<sub>2</sub>P/GC electrode also exhibited instability during the chronoamperometry tests; with a current decrease, losing all the catalytic activity that may have resulted from the material detachment of the electrode surface with the bubble production. For Ni<sub>2</sub>P/CNT/GC, Ni<sub>2</sub>P/CNT/CP, and Ni<sub>2</sub>P/GC electrodes, double layer capacitance and consequently ECSA also presented a variation during the experiments (Figs. S7–8). The ECSA values of Ni<sub>2</sub>P/CNT/GC started with 1.79 cm<sup>-2</sup> and ended with 1.66 cm<sup>-2</sup> revealing a small variance that could be attributed to a blocking of active sites due to the formation of bubbles or loss of the catalyst during the experiment. For the Ni<sub>2</sub>P/GC the same behavior was seen, starting with 0.32 cm<sup>-2</sup> and ended with 0.20 cm<sup>-2</sup>. In the Ni<sub>2</sub>P/CNT/CP case, the ECSA increased from 0.027 cm<sup>-2</sup> to 0.46 cm<sup>-2</sup> which is a large variation that may have happened due to porosity of the carbon paper.

## Conclusions

Ni<sub>2</sub>P/CNT and Ni<sub>2</sub>P were synthesized through a simpler hydrothermal route. The electrocatalysts were employed for HER and OER in acidic and alkaline media respectively. Extensive electrochemical studies were conducted to elucidate HER and OER activities of the synthesized electrocatalysts. Ni<sub>2</sub>P/CNT showed higher activity and with lower  $\eta_{10}$  of 137 mV following Volmer-Heyrovsky HER mechanism. In the case OER, Ni<sub>2</sub>P/CNT exhibited lower  $\eta_{10}$  of 360 mV and larger ECSA. Advantages of carbon support leading to improved ECSA, faster reaction kinetics and enhanced stability were demonstrated by comparing with unsupported Ni<sub>2</sub>P.

Thus, the hydrothermally synthesized Ni<sub>2</sub>P/CNT can be a better alternative for use as a platinum-free electrocatalyst that can be applied in the water splitting process. Further experiments to demonstrate HER and OER activities of Ni<sub>2</sub>P/CNT in the same electrolyte are underway.

## Author contributions

The manuscript was written through contributions of all authors. All authors have given approval to the final version of the manuscript.

## Declaration of competing interest

The authors declare that they have no known competing financial interests or personal relationships that could have appeared to influence the work reported in this paper.

## Acknowledgments

We are grateful to LAMAS – Laboratório Multiusuário de Análise de Superfícies from UFRGS for the XPS facilities. G.M. wishes to thank CNPq (grants 303351/2018-7 and 405742/2018-

5), Fundect-MS (grant 59/300.184/2016), and CAPES-PRINT (grant 88881.311799/2018-01) for their financial support. B.K.M. and L.S.B. thank CAPES for the fellowship. This study was financed in part by the Coordenacão de Aperfeiçoamento de Pessoal de Nível Superior – Brasil (CAPES) – Finance Code 001. JM and KP thank Thiruvalluvar University authorities for providing facilities.

## Appendix A. Supplementary data

Supplementary data to this article can be found online at <https://doi.org/10.1016/j.ijhydene.2020.09.263>.

## REFERENCES

- [1] Tiwari JN, Sultan S, Myung CW, Yoon T, Li N, Ha M, Harzandi AM, Park HJ, Kim DY, Chandrasekaran SS, Lee WG, Vij V, Kang H, Shin TJ, Shin HS, Lee G, Lee Z, Kim KS. Multicomponent electrocatalyst with ultralow Pt loading and high hydrogen evolution activity. *Nat. Energy*. 2018;3:773–82. <https://doi.org/10.1038/s41560-018-0209-x>.
- [2] Turner JA. Sustainable hydrogen production. *Science* 2004;305:972–4. <https://doi.org/10.1126/science.1103197>.
- [3] Cabán-Acevedo M, Stone ML, Schmidt JR, Thomas JG, Ding Q, Chang H-C, Tsai M-L, He J-H, Jin S. Efficient hydrogen evolution catalysis using ternary pyrite-type cobalt phosphosulphide. *Nat Mater* 2015;14:1245–51. <https://doi.org/10.1038/nmat4410>.
- [4] Luo J, Im J-H, Mayer MT, Schreier M, Nazeeruddin MK, Park N-G, Tilley SD, Fan HJ, Gratzel M. Water photolysis at 12.3% efficiency via perovskite photovoltaics and earth-abundant catalysts. *Science* 2014;345:1593–6. <https://doi.org/10.1126/science.1258307>.
- [5] Pu Z, Zhao J, Amiinu IS, Li W, Wang M, He D, Mu S. A universal synthesis strategy for P-rich noble metal diphosphide-based electrocatalysts for the hydrogen evolution reaction. *Energy Environ Sci* 2019;12:952–7. <https://doi.org/10.1039/C9EE00197B>.
- [6] Theerthagiri J, Cardoso ESF, Fortunato GV, Casagrande GA, Senthilkumar B, Madhavan J, Maia G. Highly electroactive Ni pyrophosphate/Pt catalyst toward hydrogen evolution reaction. *ACS Appl Mater Interfaces* 2019;11:4969–82. <https://doi.org/10.1021/acsami.8b18153>.
- [7] Roger I, Shipman MA, Symes MD. Earth-abundant catalysts for electrochemical and photoelectrochemical water splitting. *Nat. Rev. Chem.* 2017;1:3. <https://doi.org/10.1038/s41570-016-0003>.
- [8] Mu J, Li J, Yang E-C, Zhao X-J. Three-dimensional hierarchical nickel cobalt phosphide nanoflowers as an efficient electrocatalyst for the hydrogen evolution reaction under both acidic and alkaline conditions. *ACS Appl Energy Mater* 2018;1:3742–51. <https://doi.org/10.1021/acsam.8b00540>.
- [9] Ding Q, Song B, Xu P, Jin S. Efficient electrocatalytic and photoelectrochemical hydrogen generation using MoS<sub>2</sub> and related compounds. *Inside Chem* 2016;1:699–726. <https://doi.org/10.1016/j.chempr.2016.10.007>.
- [10] Landman A, Dotan H, Shter GE, Wullenkord M, Houaijia A, Maljusch A, Grader GS, Rothschild A. Photoelectrochemical water splitting in separate oxygen and hydrogen cells. *Nat Mater* 2017;16:646–51. <https://doi.org/10.1038/nmat4876>.
- [11] Fabbri E, Nachtegaal M, Binninger T, Cheng X, Kim B-J, Durst J, Bozza F, Graule T, Schäublin R, Wiles L, Pertoso M,

- Danilovic N, Ayers KE, Schmidt TJ. Dynamic surface self-reconstruction is the key of highly active perovskite nanoelectrocatalysts for water splitting. *Nat Mater* 2017;16:925–31. <https://doi.org/10.1038/nmat4938>.
- [12] Wang L, Li Y, Xia M, Li Z, Chen Z, Ma Z, Qin X, Shao G. Ni nanoparticles supported on graphene layers: an excellent 3D electrode for hydrogen evolution reaction in alkaline solution. *J Power Sources* 2017;347:220–8. <https://doi.org/10.1016/j.jpowsour.2017.02.017>.
- [13] Nazir H, Louis C, Jose S, Prakash J, Muthuswamy N, Buan MEM, Flox C, Chavan S, Shi X, Kauranen P, Kallio T, Maia G, Tammeveski K, Lymeropoulos N, Carcadea E, Veziroglu E, Iranzo A, Kannan AM. Is the H<sub>2</sub> economy realizable in the foreseeable future? Part I: H<sub>2</sub> production methods. *Int J Hydrogen Energy* 2020;45:13777–88. <https://doi.org/10.1016/j.ijhydene.2020.03.092>.
- [14] Nazir H, Muthuswamy N, Louis C, Jose S, Prakash J, Buan ME, Flox C, Chavan S, Shi X, Kauranen P, Kallio T, Maia G, Tammeveski K, Lymeropoulos N, Carcadea E, Veziroglu E, Iranzo A, Kannan AM. Is the H<sub>2</sub> economy realizable in the foreseeable future? Part II: H<sub>2</sub> storage, transportation, and distribution. *Int J Hydrogen Energy* 2020;45:20693–708. <https://doi.org/10.1016/j.ijhydene.2020.05.241>.
- [15] Pan Y, Chen Y, Lin Y, Cui P, Sun K, Liu Y, Liu C. Cobalt nickel phosphide nanoparticles decorated carbon nanotubes as advanced hybrid catalysts for hydrogen evolution. *J Mater Chem A* 2016;4:14675–86. <https://doi.org/10.1039/c6ta06975d>.
- [16] Popczun EJ, McKone JR, Read CG, Biacchi AJ, Wiltrot AM, Lewis NS, Schaa RE. Nanostructured nickel phosphide as an electrocatalyst for the hydrogen evolution reaction. *J Am Chem Soc* 2013;135:9267–70. <https://doi.org/10.1021/ja403440e>.
- [17] Menezes PW, Indra A, Das C, Walter C, Göbel C, Gutkin V, Schmeißer D, Driess M. Uncovering the Nature of Active Species of Nickel Phosphide Catalysts in High-Performance Electrochemical Overall Water Splitting. *ACS Catal* 2017;7:103–9. <https://doi.org/10.1021/acscatal.6b02666>.
- [18] Zhu Y-P, Liu Y-P, Ren T-Z, Yuan Z-Y. Self-supported cobalt phosphide mesoporous nanorod arrays: a flexible and bifunctional electrode for highly active electrocatalytic water reduction and oxidation. *Adv Funct Mater* 2015;25:7337–47. <https://doi.org/10.1002/adfm.201503666>.
- [19] Murthy AP, Theerthagiri J, Premnath K, Madhavan J, Murugan K. Single-step electrodeposited molybdenum incorporated nickel sulfide thin films from low-cost precursors as highly efficient hydrogen evolution electrocatalysts in acid medium. *J Phys Chem C* 2017;121:11108–16. <https://doi.org/10.1021/acs.jpcc.7b02088>.
- [20] Zhang Y, Wang G, Jin Z. An orderly assembled g-C<sub>3</sub>N<sub>4</sub>, rGO and Ni<sub>2</sub>P photocatalyst for efficient hydrogen evolution. *Int J Hydrogen Energy* 2019;44:10316–27. <https://doi.org/10.1016/j.ijhydene.2019.03.006>.
- [21] Murthy AP, Theerthagiri J, Madhavan J, Murugan K. Highly active MoS<sub>2</sub>/carbon electrocatalysts for the hydrogen evolution reaction – insight into the effect of the internal resistance and roughness factor on the Tafel slope. *Phys Chem Chem Phys* 2017;19. <https://doi.org/10.1039/C6CP07416B>. 1988–1998.
- [22] Dionigi F, Reier T, Pawolek Z, Gliech M, Strasser P. Design criteria, operating conditions, and nickel-iron hydroxide catalyst materials for selective seawater electrolysis. *ChemSusChem* 2016;9:962–72. <https://doi.org/10.1002/cssc.201501581>.
- [23] Ma M, Zhu G, Xie F, Qu F, Liu Z, Du G, Asiri AM, Yao Y, Sun X. Homologous catalysts based on Fe-doped CoP nanoarrays for high- performance full water splitting under benign conditions. *Chem.SusChem* 2017;3:188–92. <https://doi.org/10.1002/cssc.201700693>.
- [24] Wang X, Kolen'ko YV, Liu L. Direct solvothermal phosphorization of nickel foam to fabricate integrated Ni<sub>2</sub>P-nanorods/Ni electrodes for efficient electrocatalytic hydrogen evolution. *Chem Commun* 2015;51:6738–41. <https://doi.org/10.1039/C5CC00370A>.
- [25] Huang Z, Chen Z, Chen Z, Lv C, Humphrey MG, Zhang C. Cobalt phosphide nanorods as an efficient electrocatalyst for the hydrogen evolution reaction. *Nanomater Energy* 2014;9:373–82. <https://doi.org/10.1016/j.nanoen.2014.08.013>.
- [26] Liang H, Gandi AN, Anjum DH, Wang X, Schwingenschlögl U, Alshareef HN. Plasma-assisted synthesis of NiCoP for efficient overall water splitting. *Nano Lett* 2016;16:7718–25. <https://doi.org/10.1021/acs.nanolett.6b03803>.
- [27] Jiang P, Liu Q, Liang Y, Tian J, Asiri AM, Sun X. A cost-effective 3D hydrogen evolution cathode with high catalytic activity: FeP nanowire array as the active phase. *Angew Chem Int Ed* 2014;53:12855–9. <https://doi.org/10.1002/anie.201406848>.
- [28] Tian J, Liu Q, Cheng N, Asiri AM, Sun X. Self-supported Cu<sub>3</sub>P nanowire arrays as an integrated high-performance three-dimensional cathode for generating hydrogen from water. *Angew Chem Int Ed* 2014;53:9577–81. <https://doi.org/10.1002/anie.201403842>.
- [29] Xing Z, Liu Q, Asiri AM, Sun X. Closely interconnected network of molybdenum phosphide nanoparticles: a highly efficient electrocatalyst for generating hydrogen from water. *Adv Mater* 2014;26:5702–7. <https://doi.org/10.1002/adma.201401692>.
- [30] Shi Y, Zhang B. Recent advances in transition metal phosphide nanomaterials: synthesis and applications in hydrogen evolution reaction. *Chem Soc Rev* 2016;45:1529–41. <https://doi.org/10.1039/C5CS00434A>.
- [31] Tian J, Liu Q, Asiri AM, Sun X. Self-supported nanoporous cobalt phosphide nanowire arrays: an efficient 3D hydrogen-evolving cathode over the wide range of pH 0–14. *J Am Chem Soc* 2014;136:7587–90. <https://doi.org/10.1021/ja503372r>.
- [32] Stern L-A, Feng L, Song F, Hu X. Ni<sub>2</sub>P as a Janus catalyst for water splitting: the oxygen evolution activity of Ni<sub>2</sub>P nanoparticles. *Energy Environ Sci* 2015;8:2347–51. <https://doi.org/10.1039/C5EE0115H>.
- [33] Li Z, Dou X, Zhao Y, Wu C. Enhanced oxygen evolution reaction of metallic nickel phosphide nanosheets by surface modification. *Inorg. Chem. Front.* 2016;3:1021–7. <https://doi.org/10.1039/C6QI00078A>.
- [34] Sun H, Xu X, Yan Z, Chen X, Cheng F, Weiss PS, Chen J. Porous multishelled Ni<sub>2</sub>P hollow microspheres as an active electrocatalyst for hydrogen and oxygen evolution. *Chem Mater* 2017;29:8539–47. <https://doi.org/10.1021/acs.chemmater.7b03627>.
- [35] Yu X-Y, Feng Y, Guan B, Lou XWD, Paik U. Carbon coated porous nickel phosphides nanoplates for highly efficient oxygen evolution reaction. *Energy Environ Sci* 2016;9:1246–50. <https://doi.org/10.1039/C6EE00100A>.
- [36] Wang X, Li W, Xiong D, Petrovykh DY, Liu L. Bifunctional nickel phosphide nanocatalysts supported on carbon fiber paper for highly efficient and stable overall water splitting. *Adv Funct Mater* 2016;26:4067–77. <https://doi.org/10.1002/adfm.201505509>.
- [37] Wang X, Li W, Xiong D, Liu L. Fast fabrication of self-supported porous nickel phosphide foam for efficient, durable oxygen evolution and overall water splitting. *J Mater Chem A* 2016;4:5639–46. <https://doi.org/10.1039/C5TA10317G>.
- [38] Wang M, Lin M, Li J, Huang L, Zhuang Z, Lin C, Zhou L, Mai L. Metal–organic framework derived carbon-confined Ni<sub>2</sub>P nanocrystals supported on graphene for an efficient oxygen evolution reaction. *Chem Commun* 2017;53:8372–5. <https://doi.org/10.1039/C7CC03558F>.

- [39] Xu J, Li J, Xiong D, Zhang B, Liu Y, Wu K-H, Amorim I, i Li W, Liu L. Trends in activity for the oxygen evolution reaction on transition metal ( $M = Fe, Co, Ni$ ) phosphide precatalysts. *Chem Sci* 2018;9:3470–6. <https://doi.org/10.1039/c7sc05033j>.
- [40] Wang X-D, Cao Y, Teng Y, Chen H-Y, Xu Y-F, Kuang D-B. Large-area synthesis of a  $Ni_2P$  honeycomb electrode for highly efficient water splitting. *ACS Appl Mater Interfaces* 2017;9:32812–9. <https://doi.org/10.1021/acsmami.7b1089>.
- [41] Murthy AP, Madhavan J, Murugan K. Recent advances in hydrogen evolution reaction catalysts on carbon/carbon-based supports in acid media. *J Power Sources* 2018;398:9–26. <https://doi.org/10.1016/j.jpowsour.2018.1007.1040>.
- [42] Ma D, Meng K, Ma J, Jia Z, Wang Y, Liu L, Qi T. The catalytic performance enhancement of  $Ni_2P$  electrocatalysts for hydrogen evolution reaction by carbon-based substrates. *Int J Hydrogen Energy* 2019;44:31960–8. <https://doi.org/10.1016/j.ijhydene.2019.10.102>.
- [43] Pan Y, Hu W, Liu D, Liu Y, Liu C. Carbon nanotubes decorated with nickel phosphide nanoparticles as efficient nanohybrid electrocatalysts for the hydrogen evolution reaction. *J Mater Chem A* 2015;3:13087–94. <https://doi.org/10.1039/c5ta02128f>.
- [44] McCrory CCL, Jung S, Peters JC, Jaramillo TF. Benchmarking heterogeneous electrocatalysts for the oxygen evolution reaction. *J Am Chem Soc* 2013;135:16977–87. <https://doi.org/10.1021/ja407115p>.
- [45] Bezerra LS, Maia G. Developing efficient catalysts for the OER and ORR using a combination of Co, Ni, and Pt oxides along with graphene nanoribbons and  $NiCo_2O_4$ . *J Mater Chem A* 2020;8:17691–705. <https://doi.org/10.1039/DO TA05908K>.
- [46] Zhou Z, Wei L, Wang Y, Karahan HE, Chen Z, Lei Y, Chen X, Zhai S, Liao X, Chen Y. Hydrogen evolution reaction activity of nickel phosphide is highly sensitive to electrolyte pH. *J Mater Chem A* 2017;5:20390–7. <https://doi.org/10.1039/C7TA06000A>.
- [47] Fortunato GV, Cardoso ESF, Martini BK, Maia G. Ti/Pt–Pd based nanocomposite: effects of metal oxides on oxygen reduction reaction. *ChemElectroChem* 2020;7:1610–8. <https://doi.org/10.1002/celc.202000268>.
- [48] Boone V, Maia G. Pt–Pd and Pt–Pd–(Cu or Fe or Co)/graphene nanoribbon nanocomposites as efficient catalysts toward the oxygen reduction reaction. *Electrochim Acta* 2017;247:19–29. <https://doi.org/10.1016/j.electacta.2017.06.160>.
- [49] Cardoso ESF, Fortunato GV, Maia G. Use of rotating ring-disk electrodes to investigate graphene nanoribbon loadings for the oxygen reduction reaction in alkaline medium. *ChemElectroChem* 2018;5:1691–701. <https://doi.org/10.1002/celc.201800331>.
- [50] Cardoso ESF, Fortunato GV, Maia G. Modification of C O. N groups for oxygen reduction reaction on an electrochemically stabilized graphene nanoribbon surface. *J Phys Chem C* 2019;123:16308–16. <https://doi.org/10.1021/acs.jpc.9b04422>.
- [51] Cardoso ESF, Fortunato GV, Palm I, Kibena-Pöldsepp E, Greco AS, Júnior JLR, Kikas A, Merisalu M, Kisand V, Sammelselg V, Tammeveski K, Maia G. Effects of N and O groups for oxygen reduction reaction on one- and two-dimensional carbonaceous materials. *Electrochim Acta* 2020;344:136052. <https://doi.org/10.1016/j.electacta.2020.136052>.
- [52] Wei C, Sun S, Mandler D, Wang X, Qiao SZ, Xu ZJ. Approaches for measuring the surface areas of metal oxide electrocatalysts for determining their intrinsic electrocatalytic activity. *Chem Soc Rev* 2019;48:2518–34. <https://doi.org/10.1039/c8cs00848e>.
- [53] Wang S, Zhang L, Li X, Li C, Zhang R, Zhang Y, Zhu H. Sponge-like nickel phosphide–carbon nanotube hybrid electrodes for efficient hydrogen evolution over a wide pH range. *Nano Res* 2016;10:415–25. <https://doi.org/10.1007/s12274-016-1301-9>.
- [54] Huo S, Yang S, Niu Q, Yang F, Song L. Synthesis of functional  $Ni_2P/CC$  catalyst and the robust performances in hydrogen evolution reaction and nitrate reduction. *Int J Hydrogen Energy* 2019;45:4015–25. <https://doi.org/10.1016/j.ijhydene.2019.11.210>.
- [55] Jin Y, Zhao C, Wang L, Jiang Q, Ji C, He X. Preparation of mesoporous  $Ni_2P$  nanobelts with high performance for electrocatalytic hydrogen evolution and supercapacitor. *Int J Hydrogen Energy* 2018;43:3697–704. <https://doi.org/10.1016/j.ijhydene.2018.01.008>.
- [56] Murthy AP, Theerthagiri J, Madhavan J. Insights on Tafel constant in the analysis of hydrogen evolution reaction. *J Phys Chem C* 2018;122:23943–9. <https://doi.org/23910.21021/acs.jpc.23948b07763>.
- [57] Jin X, Li J, Cui Y, Liu X, Wang K, Zhou Y, Yang W, Zhang X, Zhang C, Jiang X, Liu B. In-situ synthesis of porous  $Ni_2P$  nanosheets for efficient and stable hydrogen evolution reaction. *Int J Hydrogen Energy* 2019;44:5739–47. <https://doi.org/10.1016/j.ijhydene.2019.01.042>.
- [58] Parra-Puerto A, Ng KL, Fahy K, Goode AE, Ryan MP, Kucernak A. Supported transition metal phosphides: activity survey for HER, ORR, OER, and corrosion resistance in acid and alkaline electrolytes. *ACS Catal* 2019;9:11515–29. <https://doi.org/10.1021/acscatal.9b03359>.
- [59] Hao X, Jiang Z, Tian X, Hao X, Maiyalagan T, Jiang Z-J. A novel particle-in-nanoplate architecture of iron nickel phosphide intertwined with carbon nanotubes for efficient water oxidation and high-performance sodium-ion batteries. *J Alloys Compd* 2019;791:122–1230. <https://doi.org/10.1016/j.jallcom.2019.03.311>.
- [60] Zhang T, Zhu Y, Lee JY. Unconventional noble metal-free catalysts for oxygen evolution in aqueous systems. *J Mater Chem A* 2018;6:8147–58. <https://doi.org/10.1039/c8ta01363b>.
- [61] Browne MP, Mills A. Determining the importance of the electrode support and fabrication method during the initial screening process of an active catalyst for the oxygen evolution reaction. *J Mater Chem A* 2018;6:14162–9. <https://doi.org/10.1039/C8TA02908C>.
- [62] Zhang B, Qi Z, Wu Z, Lui YH, Kim TH, Tang X, Zhou L, Huang W, Hu S. Defect-Rich 2D material networks for advanced oxygen evolution catalysts. *ACS Energy Lett* 2019;4:328–36. <https://doi.org/10.1021/acsenergylett.8b02343>.
- [63] Fang Y-H, Liu Z-P. Tafel kinetics of electrocatalytic reactions: from experiment to first-principles. *ACS Catal* 2014;4:4364–76. <https://doi.org/10.1021/cs501312v>.
- [64] Voiry D, Chhowalla M, Gogotsi Y, Kotov NA, Li Y, Penner RM, Schaak RE, Weiss PS. Best practices for reporting electrocatalytic performance of nanomaterials. *ACS Nano* 2018;12:9635–8. <https://doi.org/10.1021/acsnano.8b07700>.
- [65] Li G, Anderson L, Chen Y, Pan M, Abel Chuang PY. New insights into evaluating catalyst activity and stability for oxygen evolution reactions in alkaline media. *Sustain. Energy Fuels* 2018;2:237–51. <https://doi.org/10.1039/C7SE00337D>.
- [66] Anantharaj S, Ede SR, Karthick K, Sankar SS, Sangeetha K, Karthik PE, Kundu S. Precision and correctness in the evaluation of electrocatalytic water splitting: revisiting activity parameters with a critical assessment. *Energy Environ Sci* 2018;11:744–71. <https://doi.org/10.1039/c7ee03457a>.